JOURNAL OF GEOPHYSICAL RESEARCH, VOL. 116, B12313, doi:10.1029/2011JB008650, 2011

Distinct layering in the hemispherical seismic velocity structure of Earth's upper inner core

Lauren Waszek[1] and Arwen Deuss[1]

Received 1 July 2011; revised 7 October 2011; accepted 11 October 2011; published 21 December 2011.

[1] The existence of hemispherical variation in the Earth's inner core is well-documented, but consensus has not yet been reached on its detailed structure. The uppermost layers are a region of particular importance, as they are directly linked to the growth processes and post-solidification mechanisms of the inner core. Here, we use a large PKIKP-PKiKP differential travel time residual data set to derive a model for the upper inner core, providing new constraints on its isotropic and anisotropic velocity, and the amount of scattering. We find that the eastern and western hemisphere are separated by sharp boundaries. This is incompatible with the recently proposed inner core translation model, but might be explained by differences in outer core convection and inner core solidification rates. The eastern hemisphere displays weak anisotropy of 0.5%–1.0%. The western hemisphere, on the other hand, is characterized by the presence of an isotropic upper layer with a thickness of 57.5 km, with anisotropy of 2.8% appearing at deeper depths. The boundary between the isotropic layer and the deeper anisotropy appears sharp. We also detect, for the first time, a high velocity layer at the top of the eastern hemisphere with a thickness of 30 km, which we interpret as being due to an increased amount of light elements. There appears to be no relationship between the layered structure in the two hemispheres, with abrupt changes in velocity with depth in one hemisphere without any significant change at the same depth in the other hemisphere. Our results indicate that there is a difference in composition and mineral structure between the hemispheres, resulting in differing responses to external processes.

Citation: Waszek, L., and A. Deuss (2011), Distinct layering in the hemispherical seismic velocity structure of Earth's upper inner core, *J. Geophys. Res.*, *116*, B12313, doi:10.1029/2011JB008650.

1. Introduction

[2] As the Earth cools, its solid inner core grows over time through solidification of the fluid outer core. Material from the outer core freezes onto the surface of the inner core at a rate of ~1 mm/yr [*Jacobs*, 1953; *Labrosse et al.*, 2001], resulting in an age-depth relation for the inner core, whereby deeper structure is older. As the properties at the inner core boundary (ICB) are frozen into the structure, a record of the changing environments through the Earth's past is generated. Although the thermal history of the inner core remains unclear, the seismic velocity and attenuation properties of the uppermost inner core are directly linked to processes which are unlikely to have changed significantly over the last 100 Myr. Thus, through 'peeling back' the layers of the inner core, we can unravel its most recent past [*Deguen and Cardin*, 2009].

[3] Unfortunately, the seismic velocity structure of the uppermost inner core is still a topic of debate, preventing us from making direct links with Earth's thermal history. Large scale hemispherical velocity structures [*Tanaka and Hamaguchi*, 1997; *Deuss et al.*, 2010], and an isotropic upper layer atop deeper anisotropy are consistently observed [*Song and Helmberger*, 1995; *Creager*, 1999], but consensus is yet to be reached on the details of these properties. In particular, the reported seismic velocities and the extent and strength of the layered anisotropic structure are highly variable between different studies, while the sharpness of the hemisphere boundaries also remains unclear [*Garcia and Souriau*, 2000; *Ouzounis and Creager*, 2001]. We recently determined the locations of the hemisphere boundaries as a function of depth [*Waszek et al.*, 2011] and showed that the hemispheres are compatible with slow inner core super rotation of 0.1°/Myr; here we will study the corresponding isotropic and anisotropic velocity structure of the top 100 km of the inner core.

[4] Velocity anisotropy, with the fast axis aligned in the direction of Earth's rotation axis, has been observed using both body wave and normal mode techniques. It was originally thought to be present throughout the inner core [*Poupinet et al.*, 1983; *Morelli et al.*, 1986; *Woodhouse et al.*, 1986; *Creager*, 1992; *Vinnik et al.*, 1994]. Later studies found that the strongest anisotropy is located at the center of the inner core [*Su and Dziewonski*, 1995], while the outermost regions can be considered isotropic [*Shearer*, 1994; *Song and Helmberger*, 1995]. *Tanaka and Hamaguchi*

[1]Bullard Laboratories, University of Cambridge, Cambridge, UK.

0148-0227/11/2011JB008650

[1997] discovered that the inner core displayed a hemispherical velocity structure; *Creager* [1999] subsequently showed that the upper isotropic layer is only present in the western hemisphere, with no equivalent layer in the east.

[5] Since its initial discovery, there remains much disagreement with regards to the depth extent of the isotropic layer into the western hemisphere of the inner core. Body wave studies reported thicknesses ranging from 50 km [*Shearer*, 1994; *Song and Helmberger*, 1995; *Ouzounis and Creager*, 2001; *Yu and Wen*, 2007], to 100–200 km [*Song and Helmberger*, 1998; *Garcia and Souriau*, 2000; *Creager*, 2000; *Sun and Song*, 2008], and in some cases up to even 250 km [*Su and Dziewonski*, 1995; *Song and Xu*, 2002]. This variation in observed thicknesses may be as result of lateral variations, or it may be uncertainty arising due to lack of data coverage. Early normal modes studies contradicted body wave observations; *Tromp* [1993] determined the strongest anisotropy to be located in the upper inner core. *Durek and Romanowicz* [1999] allowed for an isotropic layer of 100–200 km thick, but the more recent normal mode model by *Beghein and Trampert* [2003] contained anisotropic structure at the ICB. Most recently, *Irving and Deuss* [2011a] found that normal modes are compatible with an isotropic layer of up to 275 km thick. In order to link the thickness of the isotropic layer to the thermal structure of the inner core, we need to know its extent much more precisely.

[6] In addition, a comprehensive model detailing the hemispherical differences in the seismic velocity of the uppermost inner core has yet to be produced. The east hemisphere has consistently been observed as faster than the west, although differences in isotropic velocity have been found to range from as little as 0.5% [*Sun and Song*, 2008], to 0.8%–1% [*Tanaka and Hamaguchi*, 1997; *Niu and Wen*, 2001; *Cao and Romanowicz*, 2004], and in some studies as much as 1.5% [*Garcia*, 2002]; these differences have been detected up to depths of 800 km [*Oreshin and Vinnik*, 2004; *Irving and Deuss*, 2011b]. A low velocity uppermost layer of 40 km thickness has been detected in the equatorial regions of the eastern hemisphere [*Stroujkova and Cormier*, 2004], although *Cormier* [2007] later found that the uppermost eastern hemisphere has a high velocity and shows more scattering than the western hemisphere. Greater scattering in the eastern hemisphere is also observed by *Leyton and Koper* [2007].

[7] Another unresolved problem is that a range of anisotropic strengths has been reported for the uppermost inner core. In particular, the strength of anisotropy in the deeper western hemisphere has been observed to range from 2%–4% at depths of 100–200 km [*Creager*, 1999; *Garcia and Souriau*, 2000; *Sun and Song*, 2008], up to 8% at depths greater than 250 km [*Song and Xu*, 2002]. Furthermore, the majority of investigations described the upper layer in the western hemisphere as isotropic without clarifying whether this actually refers to 0% anisotropy [*Garcia and Souriau*, 2000; *Ouzounis and Creager*, 2001; *Yu and Wen*, 2007; *Sun and Song*, 2008]. Most studies found no layered structure in the east hemisphere [*Creager*, 1999; *Garcia and Souriau*, 2000; *Sun and Song*, 2008], which is reported to display weak anisotropy of 0.5%–1% throughout the uppermost regions [*Song and Helmberger*, 1995; *Tanaka and Hamaguchi*, 1997; *Creager*, 1999]. Conversely, *Niu and Wen* [2002] observed the top 200 km of the eastern hemisphere as isotropic, with only 0.4% anisotropy in the deeper inner core.

[8] It is imperative to place better constraints on the velocity properties of the uppermost inner core if we are to understand the origins of the hemispherical structure and the anisotropy. Two different mechanisms have been proposed; any valid process must be compatible with both the existence of hemispheres and the observed anisotropy. The hemispherical differences may arise from discrepancies in regional cooling rates causing the east hemisphere to solidify faster than the west [*Sumita and Olson*, 1999; *Aubert et al.*, 2008]. Alternatively, freezing in the west and melting in the east, accompanied by an eastward lateral translation may create hemispherical differences [*Monnereau et al.*, 2010; *Alboussiére et al.*, 2010]. Neither provides an explanation for anisotropy aligned with the Earth's rotation axis. Anisotropy can arise from two distinct categories of processes. The texture can be frozen into the material structure as the inner core grows during solidification, either because of alignment with the magnetic field [*Karato*, 1993], or with the direction of heat flow [*Bergman*, 1997]. Solidification texturing would result in strong anisotropy appearing at the top of the inner core and appears to be incompatible with an isotropic top layer. The alternate category is post-solidification texturing, arising due to deformation from thermal convection [*Jeanloz and Wenk*, 1988; *Buffett*, 2009], asymmetric growth [*Yoshida et al.*, 1996], or magnetic field stresses [*Karato*, 1999; *Buffett and Wenk*, 2001]. This would lead to deeper anisotropy beneath an isotropic upper layer. Improving our knowledge of the detailed velocity structure of the inner core is the first step to determining the processes which create distinct structures in the east and west hemispheres.

[9] The variation between previous studies in the observed velocity structure, including the thickness of the isotropic layer and strengths of anisotropy, is likely a result of a lack of data. Here, we will improve global coverage by compiling a new large data set containing all suitable events from 1990 to 2011. We will use this data set to constrain the seismic velocity of the upper 100 km of the inner core, including its layered depth structure, and also constrain any laterally varying properties. We will then use our extensive data set to derive a velocity model for each hemisphere, comprising the isotropic velocities and anisotropic strengths. With this, not only will we be able to constrain the anisotropy better than previously, we will also be able to determine the sharpness of the boundary separating the upper isotropy and lower anisotropy in the western hemisphere, and infer the causative mechanism of these properties.

2. Data and Methods

2.1. Data

[10] We study the uppermost inner core using PKIKP, a seismic body wave which travels through the mantle, outer core and into the inner core, along with reference phase PKiKP, which follows the same path as PKIKP through the mantle and outer core but instead reflects from the inner core boundary (Figure 1a). PKIKP and PKiKP have very similar paths through the crust, mantle and outer core, diverging only in the uppermost inner core. Therefore the discrepancy

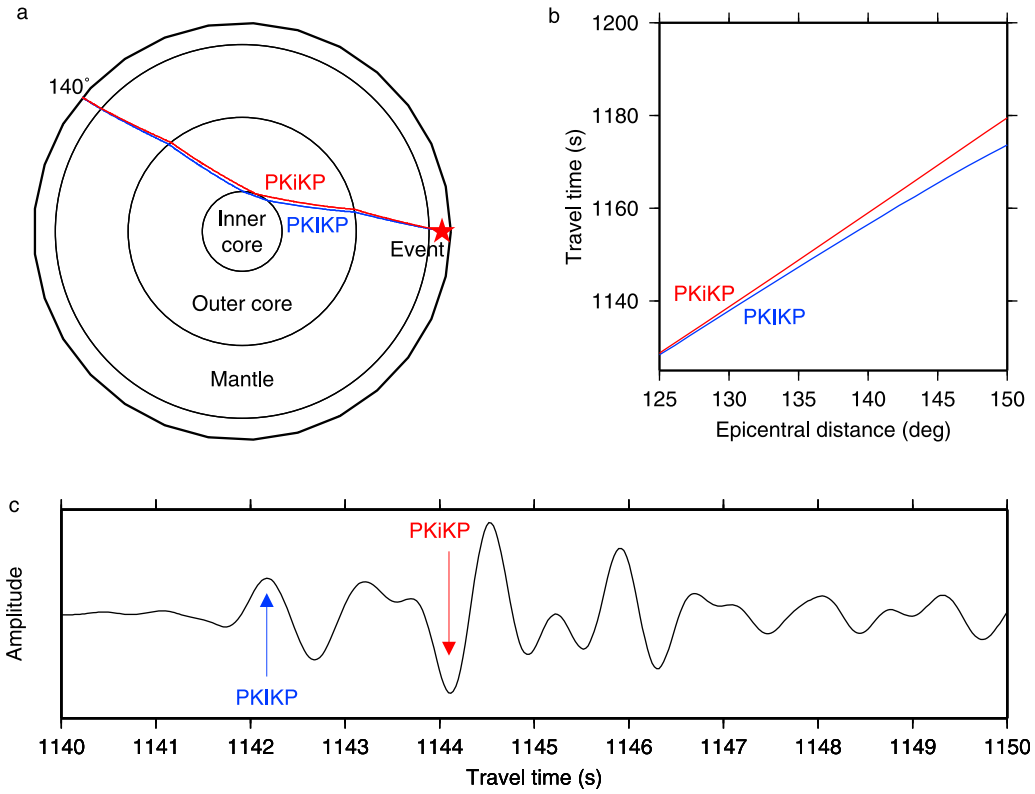

Figure 1. (a) Raypaths of PKIKP (blue) and PKiKP (red) for an event at 100 km depth. (b) Travel time curves for PKIKP and PKiKP; the two phases will be separate for an earthquake-receiver epicentral distance range of 130° – 143°. (c) Narrow band-passed displacement seismogram from an event on 5 September 2009 in Peru, observed at station AAK at an epicentral distance of 139° from the event. The first arrival is the PKIKP phase, which has traveled through the inner core; the outer core reflected phase PKiKP is observed to arrive just under 2 s later.

between actual and predicted arrival times for these phases is a result only of the velocity structure in the upper inner core differing from the seismic reference model. The ideal event for examining PKIKP and PKiKP must be able to produce observable signals which are well-separated from each other, from surface reflections such as pPKIKP and pPKiKP, and from any other outer core phases. This requires impulsive rupture mechanisms, with $5.2 < M_w < 6.3$, an event depth of 15 km or deeper and epicentral distances of 130°–143° (Figure 1b), at which PKIKP samples up to approximately 100 km deep into the inner core. We filter the broadband vertical component seismic data between 0.7 and 2.0 Hz, to center on the dominant frequency of the phases at 1.0 Hz. This filter removes any higher frequency precursors to PKIKP resulting from CMB scattering, in addition to signals from lower frequency PKP-B diffraction, both of which would otherwise interfere with the PKIKP arrival and complicate picking [*Cormier*, 1999; *Thomas et al.*, 2009].

[11] Following processing, the seismograms are inspected for quality, to ensure only those with low noise levels and clearly visible phases are used. The considerably larger quantity of data available to us in comparison to previous studies allows us to select only the highest quality seismograms. The phases are then picked using a combination of cross-correlation and hand-picking techniques (Figure 1c), exploiting the property that the phases have very similar waveforms, but opposite polarities, similar to the method used by *Irving and Deuss* [2011b]. Each phase is initially picked using cross-correlation; all are visually inspected, then hand-picked if the cross-correlation is not robust enough. The measured differential travel times of PKIKP-PKiKP are compared with those predicted by seismic reference 1D Earth model AK135 [*Kennett et al.*, 1995] to obtain differential travel time residuals:

$$\delta t = (t_{PKiKP} - t_{PKIKP})_{data} - (t_{PKiKP} - t_{PKIKP})_{model} \quad (1)$$

where t_{PKiKP} is the travel time of PKiKP and t_{PKIKP} is the travel time of PKIKP. A positive travel time residual indicates that the data differential is larger than the AK135 predicted value and thus that the PKIKP phase arrives early. This translates to a higher velocity structure along the PKIKP raypath than modeled in AK135. Likewise, a negative residual corresponds to a lower velocity structure. For this analysis we attribute any regional differences observed only to the inner core and not the outer core; a recent investigation by *Cormier et al.* [2011] finds that this assumption is valid.

[12] We examined a total of 1300 events, resulting in 49095 seismograms. Processing and quality checks reduce the quantity of seismograms significantly. We expanded on the data set from *Waszek et al.* [2011], updating it to include 118 new data points so that the final data set now contains 2615 seismograms of sufficient quality from all suitable

events between 1 January 1990 and 6 April 2011. This is therefore the most extensive PKIKP-PKiKP differential travel time residual study to date.

2.2. Anisotropy Measurement and Modeling

[13] Anisotropy is detected by examining any systematic variations in travel time residuals for paths with different directions in the inner core. The direction of a raypath is described by the variable ζ, which is the angle between the raypath of PKIKP at its turning point in the inner core and the Earth's rotation axis. Polar paths are defined as those with $\zeta < 35°$, and non-polar or equatorial paths have $\zeta > 35°$. Anisotropy oriented in a direction aligned with the Earth's rotation axis will be detected as a difference in travel time residuals between the polar and equatorial raypaths.

[14] For weak anisotropy, the perturbation to the differential travel time residuals from the reference model, δt, can be written as a function of a quartic in $\cos\zeta$ [*Creager*, 1992]:

$$\delta t = a + b\cos^2\zeta + c\cos^4\zeta \tag{2}$$

where a, b and c are related to the Love coefficients [*Love*, 1927]. The equatorial direction corresponds to $\zeta = 90°$ and the polar direction to $\zeta = 0°$, thus we can determine the equatorial and polar travel time perturbations using the following equations:

$$\delta t_{eq} = a \tag{3}$$

$$\delta t_{pol} = a + b + c \tag{4}$$

where δt_{eq} is the equatorial travel time perturbation to AK135, and δt_{pol} is the polar travel time perturbation. The strength of anisotropy is subsequently obtained as the travel time difference in seconds between the polar and equatorial raypaths:

$$\delta t_{ani} = b + c \tag{5}$$

The isotropic travel time perturbation to the reference Earth model may be obtained from averaging the travel time perturbation over all directions [*Creager*, 1999]:

$$\delta t_{iso} = a + \frac{b}{3} + \frac{c}{5} \tag{6}$$

2.3. Velocity Modeling

[15] We partition our data into layers according to the PKIKP turning point below the ICB (15–30 km, 30–57.5 km and 57.5–106 km), as predicted for each raypath from TauP [*Crotwell et al.*, 2000], in order to study the changes in travel time perturbation with depth. These depth ranges are selected as they partition the data approximately equally, while also corresponding to apparently sharp discontinuities in structural properties of the inner core: at 30 km depth below the ICB in the east hemisphere, and at 57.5 km in the west hemisphere (discussed in detail later). The results for each depth layer are affected by the structure above it, which we need to account for when investigating the properties of each layer. We remove the effect of the upper structure on the deeper layers by determining the contribution from each layer sequentially. First we use PKIKP rays which travel only in the upper layer to determine the anisotropic strength and isotropic travel time perturbation in this depth range. Using these values, we then calculate and remove the contribution of the upper layer from PKIKP raypaths traveling in the middle layer. The remaining perturbation therefore results only from the middle layer. For the lowermost layer, we again remove the contributions from the upper and middle layer according to the values determined for the upper two layers; the remainder of the perturbation results only from the lower layer.

[16] From the travel time perturbations for each layer, we subsequently calculate a layered velocity structure for each hemisphere, using the relationship:

$$\frac{\delta t}{t} = \frac{\delta v}{v} \tag{7}$$

where t is the travel time of the PKIKP raypath through the relevant layer, and v is the velocity of the relevant layer in the AK135 model. We use travel times of PKIKP raypaths through the inner core as predicted by TauP [*Crotwell et al.*, 2000].

2.4. Error Analysis

[17] We use cross-validation for determining the errors on the coefficients a, b and c obtained from fitting equation (2) to the data set. This technique involves removing a random 10% of the data, and then performing the same calculations to obtain the coefficients; this process is repeated 10 times removing a different 10% of the data for each iteration. The maximum range of these coefficients provides us with an error on each of the originally calculated a, b and c coefficients.

3. Results

3.1. General Observations

[18] We first seek a preliminary overview of the velocity structure of the uppermost inner core. Figure 2 shows the PKIKP-PKiKP differential travel time residuals as a function of PKIKP turning point longitude and depth below the ICB. Both polar and equatorial paths are included. The eastern hemisphere shows a majority of positive residuals (red data points), indicating higher velocity structure than the reference model AK135, while the western hemisphere contains mainly negative residuals (blue points) as a result of lower velocity structure. We define the boundaries between the hemispheres as located at the longitude where the residuals change from mainly positive to negative, ignoring the polar paths in the deepest layer. In Figure 2, this is the point where the data points change from predominantly red to blue, and here we indicate the hemispheres boundaries with solid black lines. These locations are also contained in Table 1. Due to additional data from the boundary regions, we are able to determine improved boundary locations from those of *Waszek et al.* [2011] and narrow the location range for the east boundary in the top layer. For the ranges of values, we take the midpoint as the longitude of the boundary for Figure 2. We also observe in Figure 2 that the travel time perturbations in each hemisphere remain consistently positive (or negative) right up to the hemisphere boundaries, with negligible overlap between positive and negative residuals

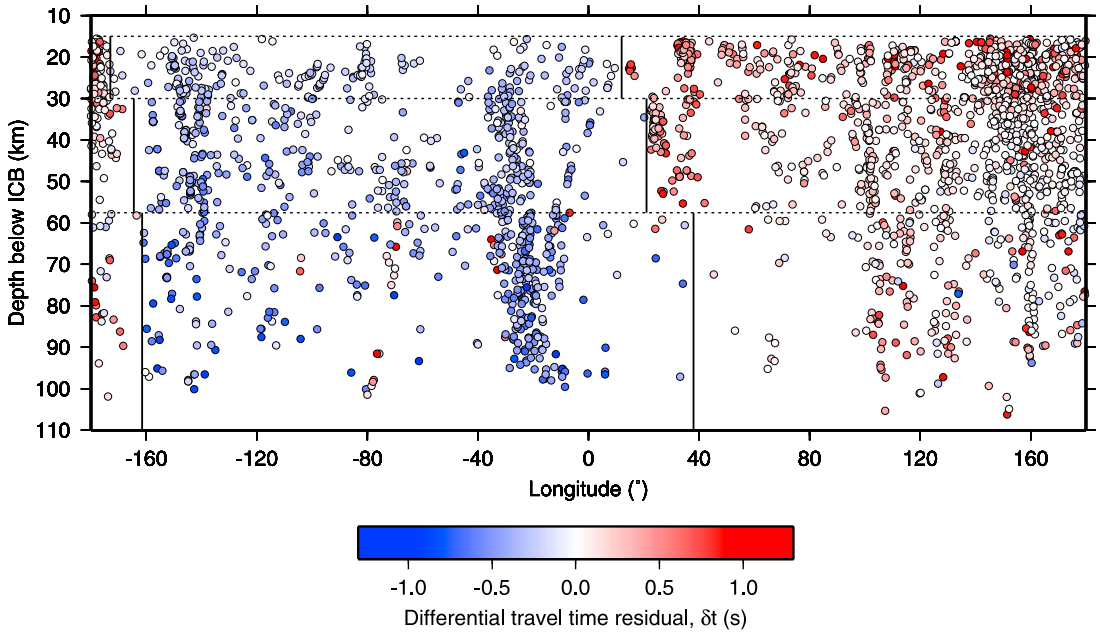

Figure 2. PKIKP-PKiKP differential travel time residuals as a function of PKIKP turning point longitude and depth below the ICB. The plot includes all paths: the red points in the deepest layer of the west hemisphere are a result of anisotropy affecting polar paths. The boundaries separating the positive residuals (red points) and negative residuals (blue points) shift eastward with increasing depth; they are also observed to be sharp, revealing the transition between the two hemispheres is not gradual.

near the boundaries. This indicates that the boundaries separating the hemispheres are sharp, and remain so to all depths in the upper 100 km of the inner core.

[19] Figure 2 also provides us with some preliminary information regarding the layered velocity structures within each hemisphere. The data are partitioned according to PKIKP turning point depth below the ICB, indicated with dashed black lines at 30 km and 57.5 km depth. We first note the appearance of red data points (i.e. positive travel time residuals) in the west hemisphere at depths below 57.5 km; these correspond to anisotropy which will be discussed in section 3.4. We also note that the upper layer of the west hemisphere has predominantly very light blue data points, corresponding to a small perturbation in the velocity from AK135. The east hemisphere contains mainly light red data points, but in the upper layer we can detect a large number of darker red points, indicating a higher velocity region. We will discuss the layered velocity structure in more detail in section 3.3.

[20] Next we investigate the PKIKP-PKiKP residuals as a function of PKIKP turning longitude, partitioned according to the PKIKP turning depth below the ICB (Figure 3). In Figure 3, the anomalous fast anisotropic polar paths are omitted, and the sharp hemisphere boundaries are therefore more clearly visible than in Figure 2. We then partition the data into longitudinal bins approximately 20° wide and determine the average travel time residual for each bin (shown as larger circles). The vertical bars correspond to the standard deviation of the average residual, which is an indicator of the spread of the data points and hence reveals the amount of scattering within each hemisphere. The standard deviation is consistently larger in the east hemisphere than the west, indicating that the travel time perturbations in the eastern hemisphere are more scattered.

[21] The Fresnel zones of our PKIKP rays in the inner core are approximately 100 km in diameter, thus the average spacing of the rays and the scatter on their travel time residuals can provide information regarding heterogeneities on scale lengths of this order. The upper east hemisphere is the region which shows greatest scatter in travel time residuals; here, we find that the difference in residuals is in excess of 1 s for PKIKP raypaths separated by as little as 4 km. *Cormier* [2007] and *Leyton and Koper* [2007] observe greater scattering in PKiKP coda in the eastern hemisphere; this results from smaller-scale heterogeneities with scale lengths of the order 1–10 km. Combining their results with our observations indicates that the east hemisphere is heterogeneous at a large range of scale lengths. The scatter is smallest in the upper layer in the west hemisphere, with PKIKP raypaths separated by up to 50 km showing a difference in residuals of less than 0.2 s. The scatter in the west hemisphere increases gradually with depth; in the deepest layer, the east and west show a similar amount of scatter.

[22] There is currently insufficient suitable data available to perform detailed regional studies throughout the hemispheres;

Table 1. Longitude, or Ranges of Longitudes, of the Hemisphere Boundary With Increasing Depth Below the ICB

Depth Below ICB (km)	West Boundary	East Boundary
15–30	−173°	10°–14°
30–57.5	−169° – −160°	21°
57.5–106	−161.5°	35°–41°

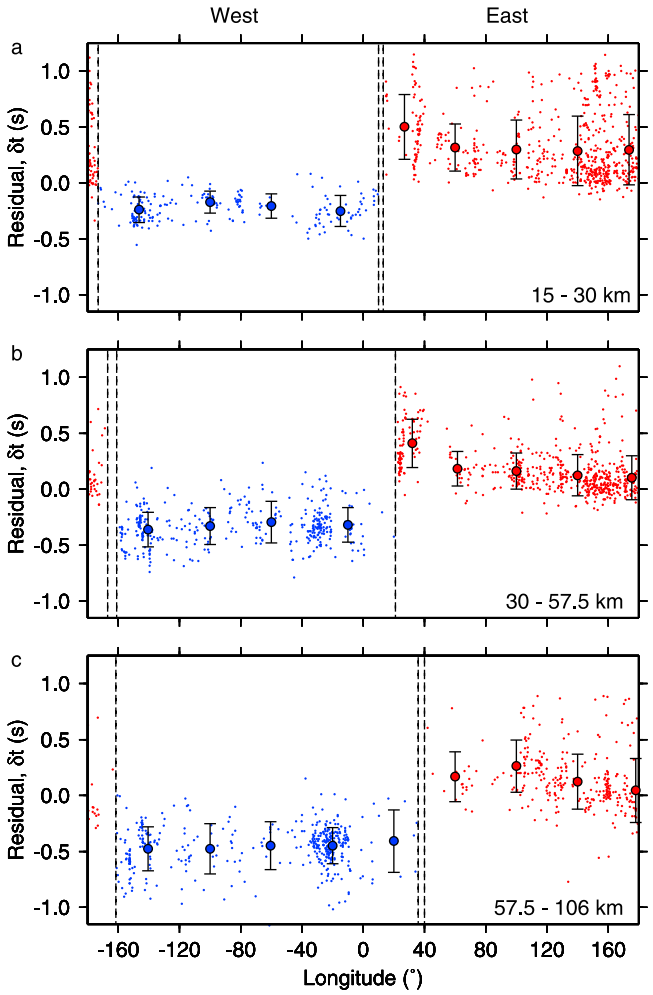

Figure 3. PKIKP-PKiKP differential travel time residuals as a function of PKIKP turning point longitude and turning depth for (a) 15–30 km below the ICB, (b) 30–57.5 km and (c) 57.5–106 km. Anomalous polar paths from the deepest data are omitted. Vertical dashed lines indicate the hemisphere boundaries. Red points are eastern hemisphere data, blue are west. The data are binned for ∼20° longitude (larger circles); error bars indicate the standard deviation of the average residual for each bin.

combined with an uneven spread in PKIKP raypaths this results in difficulty confirming any large-scale non-hemispherical differences. At present, we are not able to detect any regional variations in the velocity structure within the hemispheres themselves (Figure S1 of the auxiliary material).[1] We also do not find any evidence for large-scale regional variations in the scatter within the hemispheres, and find that the few locations with dense data coverage display consistent scatter throughout. However, the uneven spread in data means that we also cannot rule out the existence of smaller-scale non-hemispherical differences in both velocity and scatter, which may be detected as more data becomes available. Non-hemispherical variations were observed by *Deuss et al.* [2010] using normal modes, which are sensitive to the whole inner core and do not suffer from uneven data coverage.

[23] We finally investigate the travel time perturbations as function of ζ (Figure 4), to determine the isotropic, equatorial and polar travel time perturbations. Again, the data are separated according to PKIKP turning point depth below the ICB. We fit equation (2) to our data to obtain the coefficients *a*, *b* and *c*; the calculated curves are also contained in Figure 4 and the coefficients are in Table 2. The strength of anisotropy is related to the shape of the fitted curve: a more vertical line corresponds to weaker anisotropy.

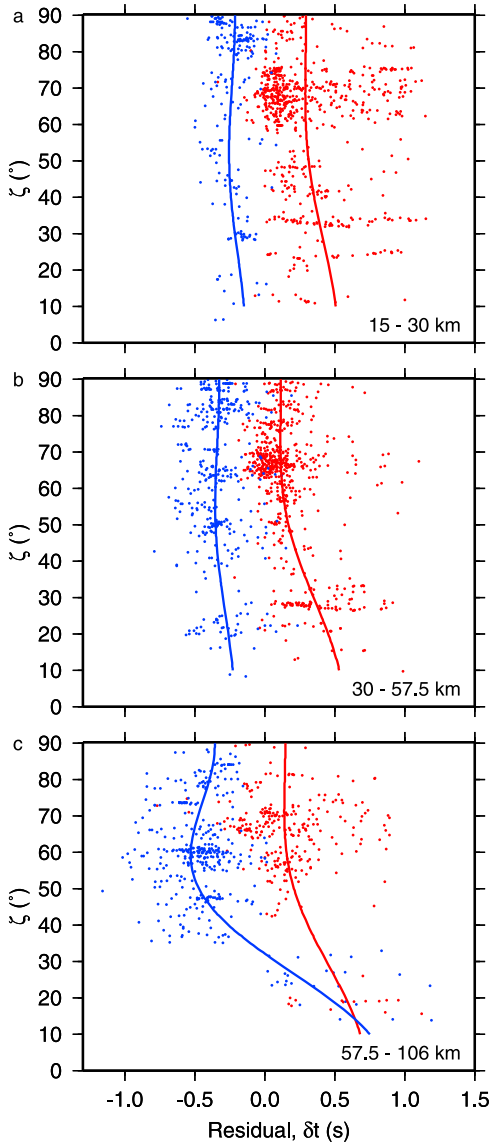

Figure 4. Differential travel time residuals as a function of ζ, the angle between the PKIKP raypath in the inner core and the Earth's rotation axis, partitioned by turning point depth: (a) 15–30 km below the ICB, (b) 30–57.5 km and (c) 57.5–106 km. The lines represent the solutions of equation (2) for the respective hemispheres; east hemisphere data are in red, west hemisphere are in blue. The hemisphere boundaries used are those which shift with depth according to *Waszek et al.* [2011].

[1]Auxiliary materials are available in the HTML. doi:10.1029/2011JB008650.

Table 2. Original Coefficients as Calculated From Equation (2) for Each Layer With Respect to Model AK135

	Depth (km)		
	15–30	30–57.5	57.5–106
West			
a (s)	−0.21 ± 0.01	−0.33 ± 0.01	−0.36 ± 0.01
b (s)	−0.22 ± 0.07	−0.19 ± 0.06	−1.32 ± 0.09
c (s)	0.30 ± 0.08	0.29 ± 0.07	2.54 ± 0.09
East			
a (s)	0.29 ± 0.02	0.11 ± 0.01	0.15 ± 0.02
b (s)	−0.08 ± 0.11	−0.09 ± 0.07	−0.15 ± 0.15
c (s)	0.31 ± 0.12	0.54 ± 0.09	0.72 ± 0.20

[24] Using Figure 4, we confirm that the velocity structure of both hemispheres consistently deviates from the reference model AK135. The western hemisphere (blue data points) contains mostly negative residuals, and thus is slower than AK135; the eastern hemisphere (red points) has predominantly positive residuals and is therefore faster. These differences persist over all three layers. It is clear in Figure 4 that the uppermost layer of the eastern hemisphere (Figure 4a) has larger travel time perturbations than the deeper regions (Figures 4b and 4c), indicating a higher velocity top layer. We also observe that the two upper layers of the inner core show weak anisotropy in both hemispheres, while only the deeper western hemisphere is strongly anisotropic.

3.2. Sharpness of Hemisphere Boundaries

[25] The sharpness of the hemisphere boundaries is an important issue in determining the mechanism responsible for the hemispherical differences. We have already discussed that the hemisphere boundaries shift eastward with depth, as was also observed by *Waszek et al.* [2011]. Here, we would like to pay particular attention to the fact that the hemisphere boundaries remain consistently sharp in each depth layer, and that the hemispherical structure is distinct right up to the boundaries. A gradual shift between the structure of the two hemispheres would result in sinusoidal travel time perturbations in Figure 3. This is observed in Figure 3c for the deepest layer, but not in Figures 3a or 3b for the two top layers, where the residuals behave almost asymptotically toward the boundary at 10–20°E. We also find that altering the reference model from AK135 to PREM2 [*Song and Helmberger*, 1995] does not affect the apparent sharpness of the boundaries, and thus it is unlikely to be an artefact of the model used.

[26] Our extensive data set also allows us for the first time to investigate the sharpness of the hemisphere boundaries across the entire surface of the inner core. Figure 5 contains PKIKP-PKiKP travel time residuals in projections from the North and South poles. The positive travel time residuals (red points) in the fast eastern hemisphere are clearly separated from the negative residuals (blue points) of the slow western hemisphere; the boundaries are marked on Figure 5 as black lines. We observe that the boundaries remain sharp across the poles. The large quantity of data in the North pole region (Figure 5a) in particular confirms the well-defined, distinct hemispherical structure.

3.3. Layered Isotropic Velocity Structure

[27] The two hemispheres in the upper inner core display a distinct difference in isotropic velocity structure, i.e. the average velocity over all directions, which is well-documented [*Niu and Wen*, 2001; *Garcia*, 2002; *Cao and*

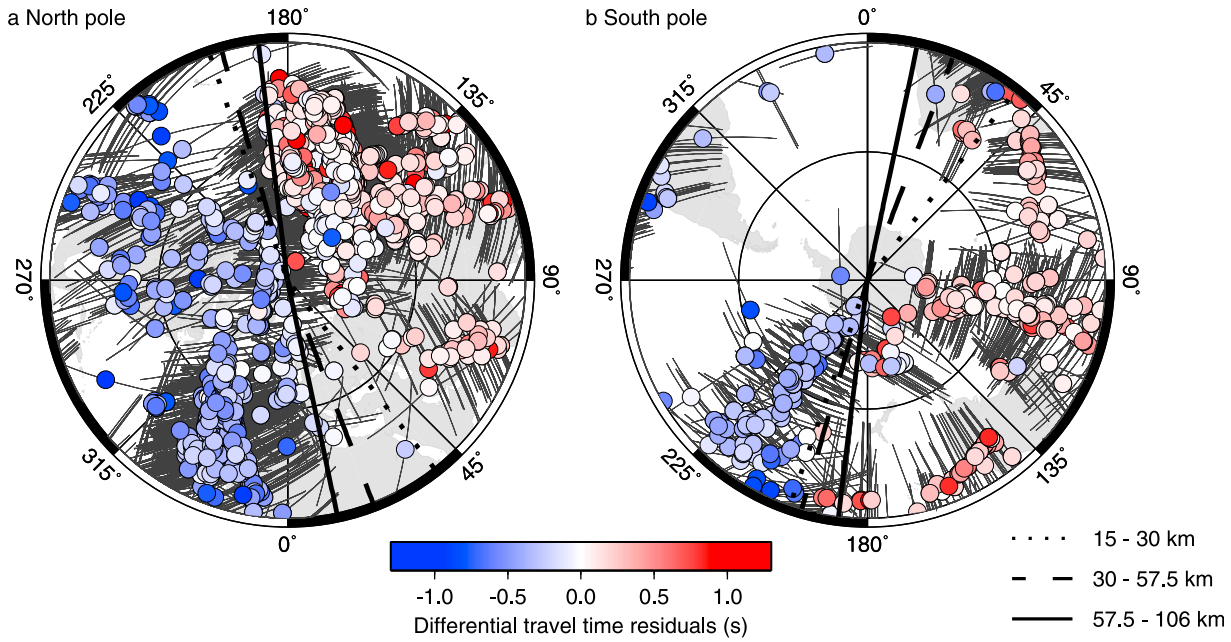

Figure 5. Maps showing PKIKP-PKiKP differential travel time residuals in the vicinity of (a) the north pole and (b) south pole. Polar paths are excluded. The circles are located at the PKIKP turning points, while the thin black lines represent the PKIKP raypaths through the inner core. The continents are projected onto the inner core boundary in grey. Hemispherical structural differences are observed to pass through the poles, with sharp boundaries.

Table 3. Depth Corrected Coefficients as Determined From Equation (2) Calculated for Each Layer With Respect to Model AK135[a]

	Depth (km)		
	15–30	30–57.5	57.5–106
West			
a (s)	−0.21 ± 0.01	−0.19 ± 0.01	−0.15 ± 0.01
b (s)	−0.22 ± 0.07	−0.05 ± 0.08	−1.20 ± 0.10
c (s)	0.30 ± 0.08	0.11 ± 0.08	2.35 ± 0.11
δv_{iso} (km s^{-1})	−0.06 ± 0.01	−0.06 ± 0.01	−0.02 ± 0.01
δv_{ani} (km s^{-1})	0.02 ± 0.03	0.02 ± 0.04	0.31 ± 0.04
δv_{ani} (%)	0.18 ± 0.25	0.19 ± 0.36	2.76 ± 0.36
West			
a (s)	0.29 ± 0.02	−0.07 ± 0.01	0.07 ± 0.02
b (s)	−0.08 ± 0.11	−0.04 ± 0.10	−0.09 ± 0.17
c (s)	0.31 ± 0.12	0.34 ± 0.12	0.38 ± 0.22
δv_{iso} (km s^{-1})	0.09 ± 0.01	0.00 ± 0.01	0.03 ± 0.02
δv_{ani} (km s^{-1})	0.06 ± 0.04	0.11 ± 0.05	0.08 ± 0.07
δv_{ani} (%)	0.55 ± 0.40	0.95 ± 0.47	0.70 ± 0.67

[a]The calculated perturbations to the isotropic velocity and the anisotropic strength as also listed.

Romanowicz, 2004; *Waszek et al.*, 2011]. We confirmed this observation and showed that the west hemisphere contains mainly negative residuals, while the east hemisphere has a majority of positive residuals (see Figures 2–5).

[28] We now use the a, b and c coefficients from Table 2 to determine the depth-corrected coefficients for each layer, using the technique described in the methods section; these depth-corrected coefficients are listed in Table 3. The perturbations to the isotropic travel time δt_{iso} are then calculated using equation (6). These values are converted to perturbations to the AK135 velocity structure δv_{iso} using predictions for the PKIKP travel time through the inner core determined from TauP. The calculated perturbations to the AK135 isotropic inner core velocity are listed in Table 3; we also list the anisotropic strength in each layer, which we will discuss in the next section. The resulting velocity model for the uppermost inner core is shown in Figure 6. The errors on the values, shown as the shaded regions around the lines, are determined using cross-validation. Larger errors for polar velocity are a result of fewer data points; the well constrained equatorial and isotropic velocities are due to the many equatorial paths studied.

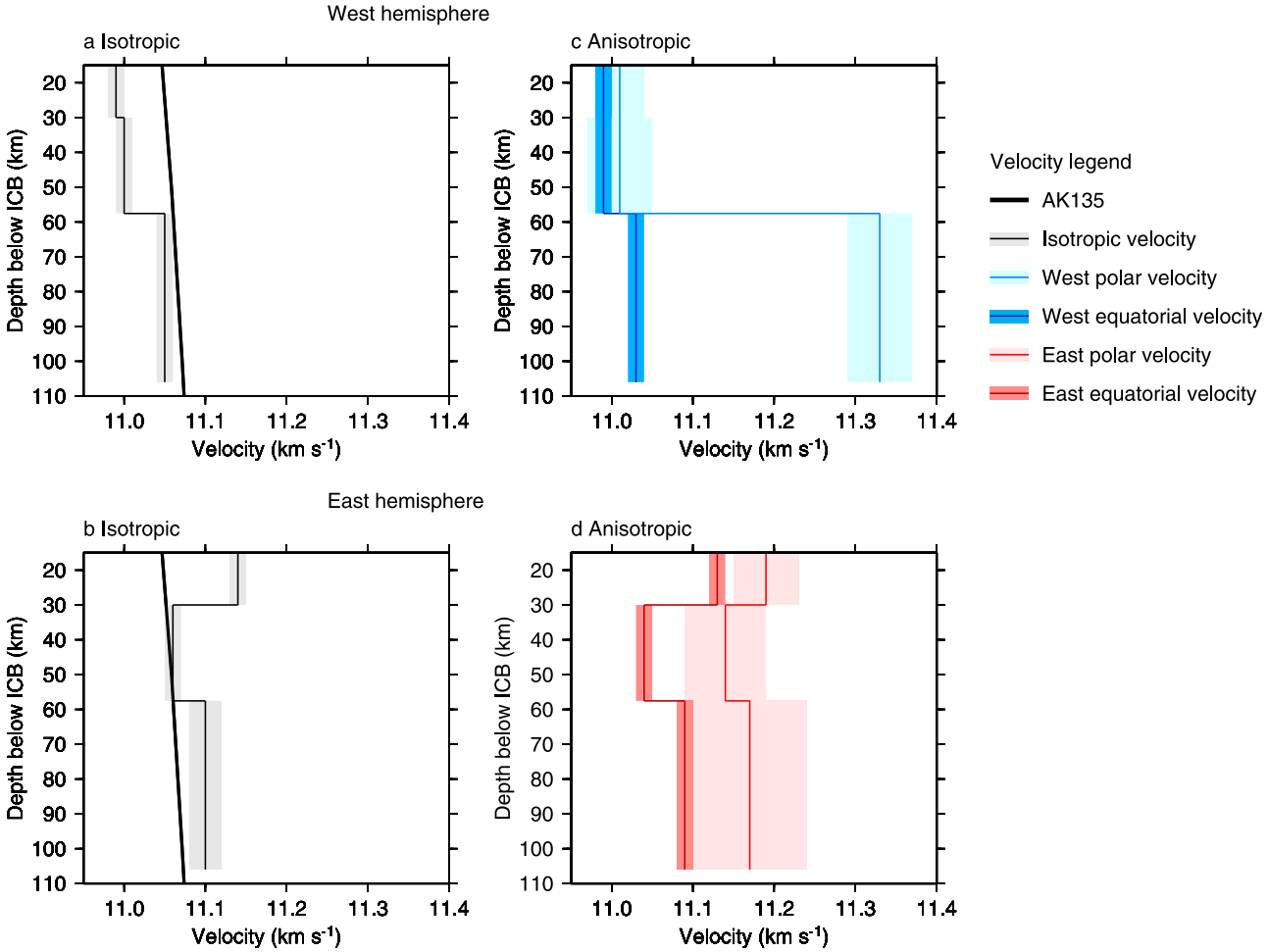

Figure 6. Calculated layered velocity models for the west and east hemispheres showing the (a, b) isotropic and (c, d) equatorial (darker shades) and polar (lighter shades) velocities. These may be compared to the reference Earth model, AK135 (thick black line). Shaded regions indicate the size of the error on the velocity models.

[29] We again find that the west hemisphere (Figure 6a) has a lower isotropic velocity than AK135 in the top 57.5 km, in agreement with the negative velocity perturbations in Figure 2. The east hemisphere (Figure 6b) has a larger isotropic velocity than AK135 in the top 30 km. This hemispherical difference in velocity gradients shows the same trend as previous observations [*Wen and Niu*, 2002; *Yu and Wen*, 2006]. We find that the isotropic velocity structure of both west and east hemisphere is tending toward that of AK135 with increasing depth.

[30] On average, we find that the difference in the isotropic velocity between the hemispheres is 0.8%, which falls within the range suggested by numerous previous studies [*Tanaka and Hamaguchi*, 1997; *Niu and Wen*, 2001; *Cao and Romanowicz*, 2004]. However, our significantly larger data set also allows us to determine a much more detailed layered velocity structure. In the upper 30 km of the inner core we find that the isotropic velocity difference between the hemispheres is 1.4%, in agreement with *Garcia* [2002]. The difference between 30–57.5 km depth decreases to 0.8%; below 57.5 km the difference is negligible at 0.2%, tending toward the preferred value of *Sun and Song* [2008]. In this deepest layer, the AK135 velocity structure lies within the error bounds of the values of both hemispheres, thus the difference in isotropic velocity is confined to the upper 57.5 km of the inner core.

[31] The most surprising find is a high velocity layer in the top 30 km of the eastern hemisphere (Figure 6b); a layer of this thickness throughout the hemisphere has not been reported in any previous studies. We see this high velocity layer in both the equatorial (Figure 6d) and isotropic velocity (Figure 6b). It is also clearly visible in Figure 2 as large differential travel time residuals in the top layer, and in Tables 2 and 3 as a higher a coefficient for the uppermost layer. The layer is separated from the deeper region (>30 km depth) by a negative jump in seismic isotropic velocity of 0.07 km s^{-1}.

3.4. Anisotropy

[32] Anisotropy in the western hemisphere, which has predominantly negative travel time residuals, is detected by the presence of anomalously positive differential travel time residuals. To determine the depth at which anisotropy appears in the western hemisphere, we examine Figure 2 for positive residuals, and in particular the depth at which these residuals first begin to appear. We find that anomalous positive residuals start appearing for paths in the western hemisphere with PKIKP turning points greater than 57.5 km depth, indicating the onset of anisotropy. We do not observe any anomalous positive residuals for paths with turning points shallower than 57.2 km depth below the ICB. Thus we locate the boundary between the second and third layer at 57.5 km depth. Of course, the exact depth is dependent on the velocity model used. But we find that by 60 km depth a significant number of anomalous polar paths have appeared between longitude of 80°W and 40°E, so there are no strong variations in isotropic layer thickness over most of the western hemisphere. For simplicity, we refer to the layer as 57.5 km thick for the remainder of the paper. We determine the fast and slow axes of this anisotropy through examining the PKIKP-PKiKP travel time residuals as a function of ζ, in Figure 4. This reveals (Figure 4c), that these anomalous fast data indeed correspond to the polar raypaths, defined as those with $\zeta < 35°$. Thus, in agreement with previous studies, the anisotropy is oriented with the fast direction aligned with the Earth's rotation axis, and symmetric about this axis.

[33] The anisotropic strength is defined as the difference between the polar and equatorial velocities in percent. Our depth-corrected results for anisotropic strength are presented in Table 3, and the subsequently determined anisotropic velocity models are contained in Figures 6c and 6d. Earlier studies did not clarify the various 'descriptive' strengths of anisotropy; here, we define strong anisotropy as being greater than 2%, weak anisotropy between 0.5%–1%, and strengths of 0.5% or less as isotropic.

[34] We find that all western polar data with PKIKP turning points deeper than 57.5 km below the ICB are strongly anisotropic (Figure 4c), with a strength of 2.8%; as a result of the large quantity of data points, this value represents the most accurate yet. Anisotropy of less than 0.2% is observed in shallower structure in the western hemisphere; 0% anisotropy is within the error ranges, revealing the presence of an isotropic layer of approximately 57.5 km thick. The increase in anisotropy to 2.8% at this depth is in good agreement with the recent study by *Yu and Wen* [2007]. The strength of deeper anisotropy we observe corresponds well with *Creager* [1999, 2000], *Garcia and Souriau* [2000], and *Sun and Song* [2008], although we have used a larger data set to improve upon their constraints on the thickness of the isotropic uppermost structure.

[35] Our thickness of 57.5 km for the upper isotropic layer in the western hemisphere corresponds well to the results found by *Song and Helmberger* [1995], *Ouzounis and Creager* [2001], and *Yu and Wen* [2007]. A number of other studies found evidence for thicker layers of 100 km [*Creager*, 2000], 150 km [*Sun and Song*, 2008] and between 100–200 km thickness [*Song and Helmberger*, 1998; *Garcia and Souriau*, 2000]; here, we have improved upon these constraints due to a significant increase in data coverage. *Sun and Song* [2008] find anisotropy in their model for depths shallower than 100 km in the western hemisphere, but argue that this is caused by model smoothing which may produce artefacts manifested as anomalously shallow anisotropy. As we observe this layer directly from our data rather than through interpretations from our model, we are confident that anisotropy in the western hemisphere starts at depths shallower than 100 km. Our results are also in good agreement with recent normal modes observations by *Irving and Deuss* [2011a]; earlier studies by *Tromp* [1993] and *Beghein and Trampert* [2003] did not allow for a thin isotropic layer, and they ignored normal mode coupling which is key in showing that an isotropic layer is possible [*Irving and Deuss*, 2011b]. We are unable to determine if there is another boundary to a further increase in anisotropic strength at 200–250 km depth below the ICB as detected by *Song and Helmberger* [1998] and *Song and Xu* [2002] as our data reaches a maximum depth of 106 km. But if a boundary exists at larger depths, it will have to be an increase in the already existing anisotropy, and it cannot be a change from isotropy to anisotropy.

[36] We observe weak anisotropy of up to 1.0% throughout most of the uppermost inner core in the eastern hemisphere (Figure 6c). The lack of more significant layering in the anisotropic structure is in good agreement with several previous observations, as is the weak strength of the anisotropy

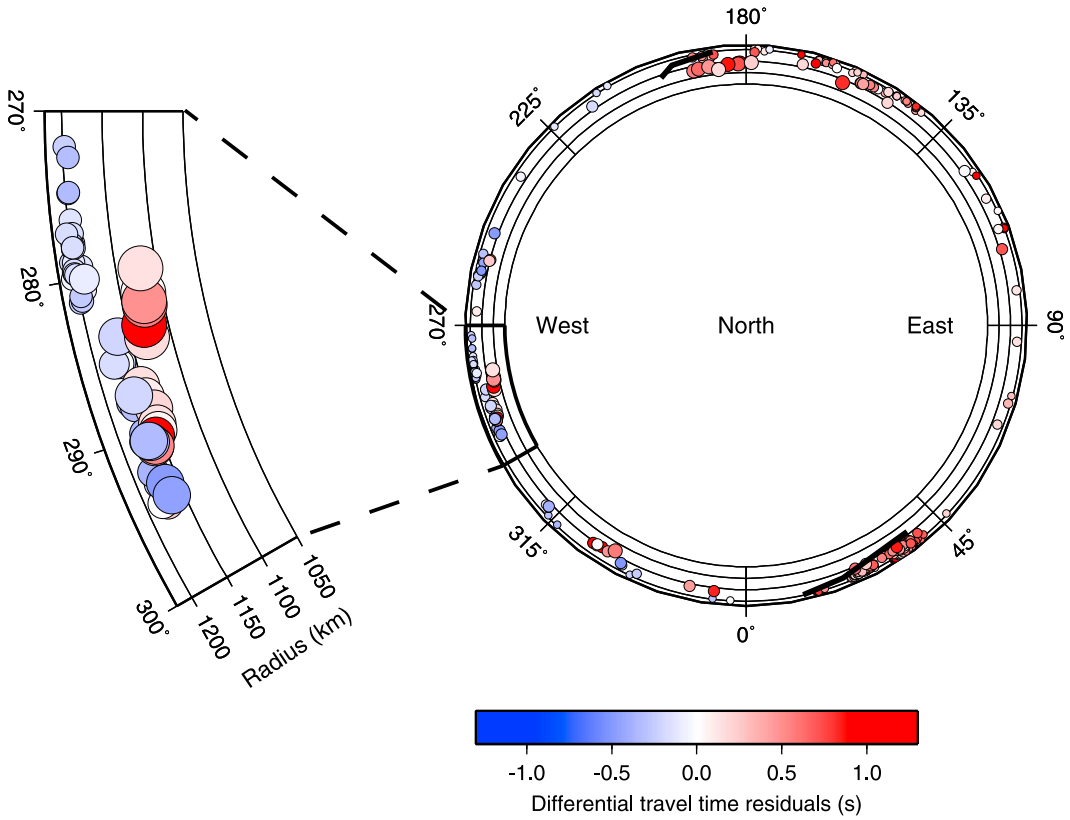

Figure 7. View from the North pole showing PKIKP-PKiKP differential travel time residuals for polar raypaths ($\zeta < 35°$) as a function of PKIKP turning point depth. Circle size equates to the size of the PKIKP Fresnel zones at their turning point. The east hemisphere shows positive residuals (red) points; the upper western hemisphere has negative (blue) residuals, while the deeper structure shows the anisotropy as positive residuals. The shifting hemisphere boundaries (Table 1) are shown with thick black lines. To the left is an enlarged portion of the west hemisphere showing the sharp change between the upper isotropic structure and lower anisotropy.

[*Creager*, 1999, 2000; *Garcia and Souriau*, 2000; *Sun and Song*, 2008]. Our results are in contrast with *Niu and Wen* [2002], who find that the eastern hemisphere is isotropic up to 200 km depth in the inner core, with only 0.4% anisotropy in the deeper parts. As our data set is significantly larger, we speculate that their smaller data set did not contain any polar paths in the required depth range to show the shallow anisotropy. It is interesting to note that the eastern hemisphere shows stronger anisotropy in the top two layers than the western hemisphere, which can be considered isotropic at these depths.

[37] Figure 7 contains only the polar paths as seen from the North pole in a slice through the equator, and shows the residuals as a function of PKIKP turning depth below the ICB. In Figure 7, the size of the circles corresponds approximately to the Fresnel zone of the PKIKP phases. Here, we observe that the polar paths from the western hemisphere jump rapidly from negative residuals (blue data points) to positive residuals (red points) at a depth of 57.5 km below the ICB; there is not a gradual change from negative to positive residuals, in agreement with Figure 2.

3.5. Waveform Modeling

[38] Using WKBJ [*Chapman*, 1976], we created synthetic seismograms to investigate the sharpness of the layers in the eastern and western hemisphere velocity models. We are particularly interested in discontinuity reflections similar to those observed by *Song and Helmberger* [1995]. In each case, we use seismograms from an event which produces ray paths which traverse one hemisphere only, and have epicentral distances corresponding to PKIKP turning points both above and below the discontinuity. For our models, synthetics with and without reflection from the discontinuity at 30 km depth in the east (PKiKP30) and 57.5 km depth in the west (PKiKP57.5) are calculated.

[39] In both hemispheres, we find a closer match between the predicted and observed travel times of PKIKP relative to PKiKP when using our updated model compared to reference model AK135. For the west hemisphere (Figures 8a and 8b), our model also results in an improvement in the waveform of PKiKP. The additional phase PKiKP57.5 can be detected in our synthetic data (Figure 8b), improving the fit of the synthetic trace compared to the observed seismogram. The fact that a reflection can be observed from this interface indicates that the change from isotropic to anisotropic structure must occur over a depth range of less than $\lambda/4$, where λ is the wavelength of the ray [*Richards*, 1972]. For our data, this corresponds to a thickness of less than 3 km for the discontinuity, which has implications for the potential mechanisms causing the anisotropy. Therefore, both the boundaries separating the hemispheres, as discussed in

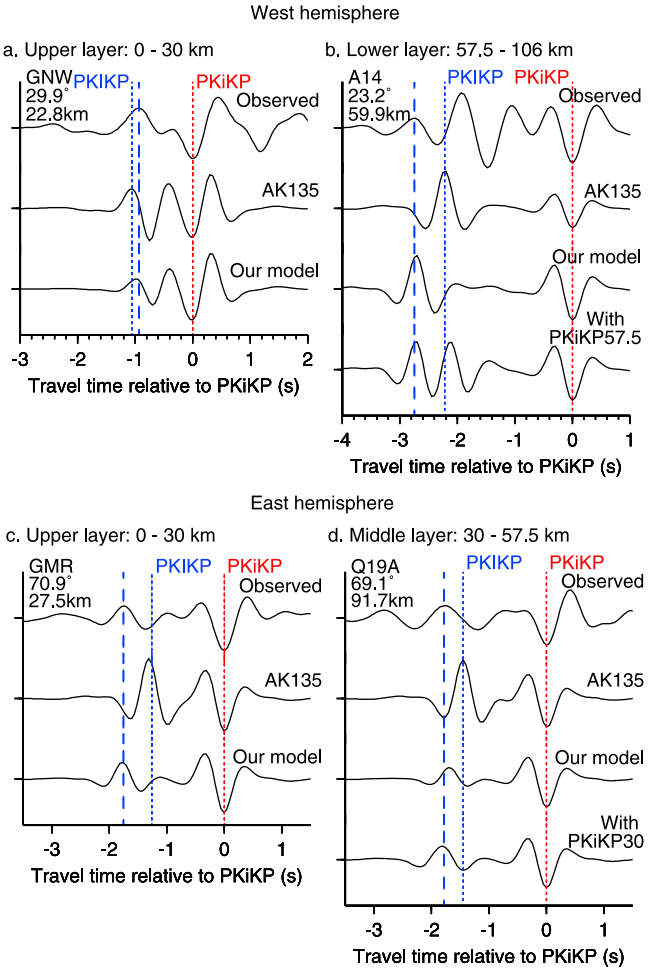

Figure 8. Observed and synthetic seismograms for PKIKP and PKiKP paths in (a, b) the west hemisphere from an event in the South Sandwich Islands on 11 September 2004, and (c, d) the east hemisphere for the Sumatra event of 10 October 2007. The station, direction ζ and PKIKP turning depth below the ICB are indicated on each panel. Synthetics for our model fit the observed data better than the reference model AK135. For the deeper paths, the phases which reflect from the interface at 30 or 57.5 km are included, denoted PKiKP30 and PKiKP57.5.

section 3.2, and the discontinuity at 57.5 km depth separating the isotropic and anisotropic velocity structures in the western hemisphere are sharp.

[40] For the east hemisphere (Figures 8c and 8d), our new model also results in an improvement in differential travel times. Using our new model alone, we observe a significantly better match in the amplitude of the PKIKP arrival, which is a result of the high velocity upper layer (Figure 8d). The addition of the reflected phase results in a slight improvement of the synthetic trace, but cannot be detected as an arrival. The smaller amplitude of the arrival means that the change is not as dramatic as that in the western hemisphere; this is expected as the velocity jump at the discontinuity is smaller.

3.6. Summary of Observations

[41] The velocity structure of the upper inner core is complicated, showing abrupt changes both laterally and with depth. The western hemisphere has an isotropic velocity lower than AK135 and displays a clear layered structure, comprised of an uppermost 57.5 km which is isotropic, and a lower layer with strong anisotropy of 2.8%. The sharp jump in anisotropy can be seen in the abrupt increase in polar velocity (Figure 6c). There is no equivalent abrupt change at this depth in the structure of the eastern hemisphere (Figure 6d). The west hemisphere shows only a small amount of scatter in the PKIKP-PKiKP travel time residuals, which increases with depth.

[42] The east hemisphere is consistently faster than reference model AK135, accompanied by considerably more scattered residuals than in the western hemisphere. It displays approximately constant weak anisotropy of less than 1.0% up to the largest depth studied of 106 km below the ICB. In this hemisphere we detect, for the first time, a high velocity layer in the upper 30 km which also shows the largest amount of scatter. At 30 km we observe an abrupt decrease in the isotropic velocity of 0.6%; the deeper structure follows AK135. The discontinuity at 30 km is noted in the east hemisphere only, with no corresponding change at this depth in the west hemisphere.

4. Discussion

4.1. Sharp Hemisphere Boundaries

[43] The seismic velocity structure of the uppermost inner core is strongly hemispherical, in both its isotropic velocity and anisotropy. Through extra data coverage in the regions near the boundaries, we are able to improve the constraints on the shifting hemisphere boundaries first reported by *Waszek et al.* [2011]. With the ever increasing quantity of seismometers in different regions of the Earth, we will be able to improve the accuracy of the boundary locations even more over time, through targeting raypaths in the appropriate regions. As can be observed in Figure 2, the hemisphere boundaries are sharp, separating distinct regions. If the difference between the hemispheres was gradual, we would expect that the PKIKP-PKiKP residuals in the boundary region would show scatter throughout a transition region between the hemispheres. Alternatively we might expect the residuals to be close to an intermediate value between the two hemispheres. On the contrary, Figures 3a and 3b show that the eastern hemisphere residuals become larger when closer to the boundary at 10–20°E, indicating that within the fabric of the inner core there are distinct jumps at the boundaries, with little overlap in the structures of the hemispheres.

[44] We find that this sharpness of the hemisphere boundaries is a global phenomenon, with a clear separation detected even in the polar regions (Figure 5). This has implications for the mechanisms which create the hemispheres, and in particular some of the recently proposed ideas. These ideas assume that the hemispheres are generated by inner core growth processes driven by large scale motion in the outer core [*Sumita and Olson*, 1999; *Aubert et al.*, 2008; *Monnereau et al.*, 2010; *Alboussiére et al.*, 2010]. The most recently proposed idea involves eastward lateral translation of the inner core as a result of melting in the eastern hemisphere and freezing in the west hemisphere [*Monnereau et al.*, 2010; *Alboussiére et al.*, 2010]. This translation process would not be able to produce sharp boundaries separating the two hemispheres; instead there would be a gradual change from western to eastern

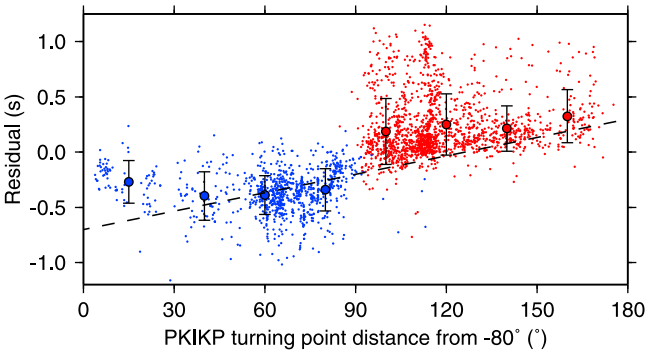

Figure 9. PKIKP-PKiKP residuals as a function of the distance between PKIKP turning point and the center of the west hemisphere (0°N, 80°W from *Monnereau et al.* [2010]). Data for the eastern hemisphere are shown in red, west are in blue; data in both hemispheres are binned (large circles). The positive correlation between travel time residual and distance from the center of the western hemisphere, taken from *Monnereau et al.* [2010], is indicated with a dashed line. Our data does not display this relationship.

structure. The residuals in the transition region between the west and east, in particular in the polar regions, would be smeared out. Furthermore, it would be expected that the travel time residuals would become more positive with increased distance of the PKIKP turning point from the center of the western hemisphere, as was shown in Figure 1d of the study by *Monnereau et al.* [2010]. Our data set contains a significantly larger amount of measurements, so we plot our data in the same manner to test this hypothesis (Figure 9). Our data does not follow the trend predicted by *Monnereau et al.* [2010]. We binned our data to investigate if any other trend exists, and found a decrease in residual with distance for the western hemisphere instead. We also observe that the boundary at 90° is sharp, and not gradual. Therefore, our data are incompatible with the theory of inner core translation as proposed by *Monnereau et al.* [2010] and *Alboussiére et al.* [2010].

[45] Another currently favored idea suggests that the hemispheres arise as a result of different cooling rates in the east and west hemispheres [*Sumita and Olson*, 1999; *Aubert et al.*, 2008]. Thermochemical coupling with the mantle creates stronger heat flow across the core-mantle boundary in the east, causing hemispherical differences in convection rates of the outer core. As a consequence, faster solidification in the east leads to less texture, weaker anisotropy, stronger attenuation and a larger isotropic velocity in the eastern hemisphere [*Aubert et al.*, 2008]. However, the large-scale solidification processes described by *Aubert et al.* [2008] do not show a sharp boundary between the east and west hemisphere. While *Cormier* [2007, 2009] suggest that lateral differences in crystallization rates may be able to produce smaller-scale variation, it is still unclear how such sharp boundaries can be produced.

[46] The difference between the hemispheres may also be historical in origin [*Tanaka and Hamaguchi*, 1997], but must currently be maintained by outer core processes as outlined above. However, the mechanism which generates the sharp hemisphere boundaries remains unclear, much in the same way as the mechanism which produces the difference between the continents and the oceans on the Earth's surface.

4.2. Velocity Structure

[47] We observe the presence of distinct layering with depth in each hemisphere, with no apparent relationship between the structures. The west hemisphere displays an abrupt change at approximately 57.5 km below the ICB, from an isotropic upper structure to deeper anisotropy. We do not observe any such change at this depth in the east hemisphere. Similarly, we detect a high velocity layer in the uppermost east hemisphere, up to depths below the ICB of 30 km, at which point there is a negative jump in isotropic seismic velocity. The west hemisphere does not display any abrupt change at this depth. This would indicate that a mechanism acting on the inner core can produce an observable change in one hemisphere, but have no effect on the other. Therefore it appears that seismic isotropic velocity and anisotropic structures in the two hemispheres are possibly independent, with the response of the material to external mechanisms differing between hemispheres.

[48] The high velocity and strongly scattered upper layer of 30 km thickness in the east hemisphere has implications for the crystal organization and composition in the top of the inner core [*Cormier*, 2007; *Leyton and Koper*, 2007]. Light elements decrease the density and increase the compressional velocity of iron at high pressure [*Badro et al.*, 2007; *Antonangeli et al.*, 2010]. Therefore the high velocity layer may indicate the presence of more light elements in the top of the eastern hemisphere compared to the deeper structure. This would also indicate a higher proportion of light elements in the overlying region of the outer core, in agreement with *Yu et al.* [2005]. More light elements in the eastern outer core would lead to more vigorous convection here and therefore more random solidification of the eastern hemisphere [*Cormier*, 2007], ultimately resulting in greater scatter. Therefore, we are able to link both the high velocity and enhanced scatter in the uppermost east hemisphere to the presence of light elements. *Cormier* [2007] suggested that as a result of faster solidification in the eastern hemisphere, the longer length scales of anisotropy are oriented perpendicular to the ICB, while in the slower-cooling western hemisphere these long length scales are arranged parallel to the ICB. The resulting texture produces greater scatter in the upper eastern hemisphere, and stronger anisotropy in the west, both in excellent agreement with our observations.

[49] There are two different categories of mechanisms which can produce alignment of the anisotropy with Earth's rotation axis: it can either be frozen in during solidification, or it can be generated by post-solidification deformation. The first mechanism involves the anisotropic properties being frozen into the material structure of the inner core as it grows over time, either by aligning with the magnetic field [*Karato*, 1993] or with the direction of heat flow [*Bergman*, 1997]. This would result in anisotropy being present at the top of the inner core, and is therefore incompatible with our observation of an upper isotropic layer in the western hemisphere. However, it may be able to explain the consistent presence of weak anisotropy throughout the upper 100 km of the eastern hemisphere.

[50] The second mechanism to generate anisotropy is a post-solidification deformation, which can preferentially deform the material crystals of the inner core to create the directional-dependent velocity structure. Such a texturing

process can arise from thermal convection in the inner core [*Jeanloz and Wenk*, 1988; *Buffett*, 2009], magnetic field stresses [*Karato*, 1999; *Buffett and Wenk*, 2001], or from asymmetric growth of the inner core [*Yoshida et al.*, 1996]. This type of process could explain the appearance of anisotropy in the western hemisphere at a depth of 57.5 km below the ICB. Convection within the top of the inner core would erase any crystal alignment thereby creating an isotropic upper layer [*Deguen and Cardin*, 2009]. Alternatively, *Vočadlo et al.* [2009] proposed that an isotropic upper layer could be caused by a property of hexagonal close packed (hcp) iron, whereby close to melting temperature, the velocity along the *c*-axis tends to that in the $a - b$ plane. Previous studies had suggested that the isotropic layer may be thicker; our new measurement can be used to constrain the deformation regime in the upper inner core as a function of depth, and may be used to determine the thermal structure of the upper inner core.

[51] *Bergman et al.* [2010] proposed a third mechanism to produce anisotropic structure which may also create hemispheres, based upon eastward translation of the inner core [*Monnereau et al.*, 2010; *Alboussiére et al.*, 2010]. Annealing during this translation could result in a loss of texture from west to east, explaining the strong anisotropy in the western hemisphere and negligible in the east. However, this mechanism cannot explain the depth-dependence and the uppermost isotropic layer. Furthermore, the lack of related change in the east hemisphere at the depth at which anisotropy appears in the west hemisphere provides further evidence for hemispherical differences in the processes which create anisotropy. Also, our observation of sharp boundaries between the two hemispheres does not agree with the idea of inner core translation.

[52] The sharp velocity interfaces with depth, which we observe to be distinct in each hemisphere, suggest a combination of post-solidification texturing or deformation mechanisms which occur separately in the east and west hemispheres. External forces resulting from gravitational or electromagnetic torques would act on the entire inner core. The fact that an abrupt change in one hemisphere does not equate to an abrupt change in the other indicates that the mechanisms occur independently within each hemisphere, and there is no interaction between the two. Therefore, the forces acting on the inner core produce different effects on the material structure dependent on the hemisphere in question, which indicates contrasting crystal orientations or variations in composition such as the presence of more light elements in the east hemisphere. The isotropic upper layer we observe in the western hemisphere further supports the idea that the deeper anisotropy is due to deformation texturing, while the overall hemispherical difference in isotropic velocity is maintained by outer core flow processes. This is in good agreement with the study by *Deguen and Cardin* [2009], which suggested that the deeper anisotropy is a result of ancient deformation by the magnetic field or solidification texturing, while the isotropic structure in the upper layers is created by the current heterogeneous growth of the inner core via 'active tectonics'.

5. Conclusions

[53] We find that the seismic velocity structure of the uppermost inner core displays strong hemispherical structure, separated into distinct east and west regions which differ in isotropic velocity, anisotropy, and layered velocity structure. We observed sharp boundaries separating the hemispheres, with no overlap between the structure of the two regions. The sharp boundaries are incompatible with the inner core translation idea of *Monnereau et al.* [2010] and *Alboussiére et al.* [2010].

[54] We confirm the presence of an isotropic upper layer in the west hemisphere, and determine its thickness as 57.5 km. The deepest west displays 2.8% anisotropy. The boundary between the isotropic layer and the deeper anisotropy appears to be sharp, indicating that the underlying anisotropy is a result of a post-solidification deformation mechanism which occurs at a depth of 57.5 km below the ICB.

[55] We also observe the presence of a high velocity layer in the top 30 km of the east hemisphere. This previously undetected high velocity lid shows a great amount of scatter, and is separated from the deeper structure by an abrupt interface. It is likely that the high velocity layer is caused by a higher concentration of light element concentration at the top of the eastern hemisphere. We do not observe a corresponding change in the west hemisphere.

[56] There appears to be a lack of relationship between the layered structure of hemispheres. An abrupt change in velocity in one hemisphere does not equate to any sharp change in the other. We observe the different structures right up to the hemisphere boundaries, with no gradual change or overlap between them. This indicates that the forces producing the processes that generate the different velocity properties act differently in each hemisphere. We suggest that the continuing difference between the hemispheres is caused by solidification processes in the outer core leading to different texturing and light element concentrations in the two hemispheres. However, the actual mechanism which is responsible for the sharp boundary between the two hemispheres currently remains unclear.

[57] **Acknowledgments.** The research was funded by the European Research Council under the European Community's Seventh Framework Programme (FP7/2007-2013)/ERC grant 204995. We thank Elizabeth Day, Jessica Irving, and Vernon Cormier, in addition to an anonymous reviewer, for helpful and constructive comments.

References

Alboussiére, T., R. Deguen, and M. Melzani (2010), Melting-induced stratification above the Earth's inner core due to convective translation, *Nature*, *466*, 744–747.

Antonangeli, D., J. Siebert, J. Badro, D. Farber, G. Fiquet, G. Morard, and F. Ryerson (2010), Composition of the Earth's inner core from high-pressure sound velocity measurements in Fe-Ni-Si alloys, *Earth Planet. Sci. Lett.*, *295*, 292–296.

Aubert, J., H. Amit, G. Hulot, and P. Olson (2008), Thermochemical flows couple the Earth's inner core growth to mantle heterogeneity, *Nature*, *454*, 758–762.

Badro, J., G. Fiquet, F. Guyot, E. Gregoryanz, F. Occelli, D. Antonangeli, and M. d'Astuto (2007), Effect of light elements on the sound velocities in solid iron: Implications for the composition of Earth's core, *Earth Planet. Sci. Lett.*, *254*, 233–238.

Beghein, C., and J. Trampert (2003), Robust normal mode constraints on inner core anisotropy from model space search, *Science*, *299*, 552–555.

Bergman, M. (1997), Measurements of electric anisotropy due to solidification texturing and the implications for the Earth's inner core, *Nature*, *389*, 60–63.

Bergman, M., D. Lewis, I. Myint, L. Slivka, S. Karato, and A. Abreu (2010), Grain growth and loss of texture during annealing of alloys, and the translation of Earth's inner core, *Geophys. Res. Lett.*, *37*, L22313, doi:10.1029/2010GL045103.

Buffett, B. (2009), Onset and orientation of convection in the inner core, *Geophys. J. Int.*, *179*, 711–719.
Buffett, B., and H. Wenk (2001), Texturing of the Earth's inner core by Maxwell stresses, *Nature*, *413*, 60–63.
Cao, A., and B. Romanowicz (2004), Hemispherical transition of seismic attenuation at the top of the Earth's inner core, *Earth Planet. Sci. Lett.*, *228*, 243–253.
Chapman, C. (1976), A first motion alternative to geometrical ray theory, *Geophys. Res. Lett.*, *3*, 153–156.
Cormier, V. (1999), Anisotropy of heterogeneity scale lengths in the lower mantle from PKIKP precursors, *Geophys. J. Int.*, *136*, 373–384.
Cormier, V. (2007), Texture of the uppermost inner core from forward- and back-scattered seismic waves, *Earth Planet. Sci. Lett.*, *258*, 442–453.
Cormier, V. (2009), A glassy lowermost outer core, *Geophys. J. Int.*, *179*, 374–380.
Cormier, V., J. Attanayake, and K. He (2011), Inner core freezing and melting: Constraints from seismic body waves, *Phys. Earth Planet. Int.*, in press.
Creager, K. (1992), Anisotropy of the inner core from differential travel times of the phases PKP and PKIKP, *Nature*, *356*, 309–314.
Creager, K. (1999), Large-scale variations in inner core anisotropy, *J. Geophys. Res.*, *104*, 23,127–23,139.
Creager, K. (2000), Inner core anisotropy and rotation, in *Earth's Deep Interior: Mineral Physics and Tomography From the Atomic to the Global Scale*, *Geophys. Monogr. Ser.*, vol. 117, edited by S. Karato et al., pp. 89–114, AGU, Washington, D. C., doi:10.1029/GM117p0089.
Crotwell, H., T. Owens, and J. Ritsema (2000), The TauP Toolkit: Flexible seismic travel-time and raypath utilities, *Seismol. Res. Lett.*, *70*, 154–160.
Deguen, R., and P. Cardin (2009), Tectonic history of the Earth's inner core preserved in its seismic structure, *Nat. Geosci.*, *2*, 419–422.
Deuss, A., J. Irving, and J. Woodhouse (2010), Regional variation of inner core anisotropy from seismic normal mode observations, *Science*, *328*, 1018–1020.
Durek, J., and B. Romanowicz (1999), Inner core anisotropy inferred by direct inversion of normal mode spectra, *Geophys. J. Int.*, *139*, 599–622.
Garcia, R. (2002), Constraints on upper inner-core structure from waveform inversion of core phases, *Geophys. J. Int.*, *150*, 651–664.
Garcia, R., and A. Souriau (2000), Inner core anisotropy and heterogeneity level, *Geophys. Res. Lett.*, *27*, 3121–3124.
Irving, J., and A. Deuss (2011a), Stratified anisotropic structure at the top of Earth's inner core: A normal mode study, *Phys. Earth Planet. Inter.*, *186*, 59–69.
Irving, J., and A. Deuss (2011b), Hemispherical structure in inner core velocity anisotropy, *J. Geophys. Res.*, *116*, B04307, doi:10.1029/2010JB007942.
Jacobs, J. (1953), The Earth's inner core, *Nature*, *172*, 297–298.
Jeanloz, R., and H. Wenk (1988), Convection and anisotropy of the inner core, *Geophys. Res. Lett.*, *15*, 72–75.
Karato, S. (1993), Inner core anisotropy due to the magnetic field-induced preferred orientation of iron, *Science*, *262*, 1708–1711.
Karato, S. (1999), Seismic anisotropy of the Earth's inner core resulting from flow induced by Maxwell stresses, *Nature*, *402*, 871–873.
Kennett, B., E. Engdahl, and R. Buland (1995), Constraints on seismic velocities in the Earth from travel times, *Geophys. J. Int.*, *122*, 108–124.
Labrosse, S., J. Poirier, and J. Le Mouël (2001), The age of the inner core, *Earth Planet. Sci. Lett.*, *190*, 111–123.
Leyton, F., and K. Koper (2007), Using PKiKP coda to determine inner core structure: 2. Determination of Qc, *J. Geophys. Res.*, *112*, B05317, doi:10.1029/2006JB004370.
Love, A. (1927), *A Treatise on the Mathematical Theory of Elasticity*, Cambridge Univ. Press, New York.
Monnereau, M., M. Calvet, L. Margerin, and A. Souriau (2010), Lopsided growth of Earth's inner core, *Science*, *328*, 1014–1017.
Morelli, A., A. Dziewonski, and J. Woodhouse (1986), Anisotropy of the inner core inferred from PKIKP travel times, *Geophys. Res. Lett.*, *13*, 1545–1548.
Niu, F., and L. Wen (2001), Hemispherical variations in seismic velocity at the top of the Earth's inner core, *Nature*, *410*, 1081–1084.
Niu, F., and L. Wen (2002), Seismic anisotropy in the top 400 km of the inner core beneath the "eastern" hemisphere, *Geophys. Res. Lett.*, *29*(12), 1611, doi:10.1029/2001GL014118.
Oreshin, S., and L. Vinnik (2004), Heterogeneity and anisotropy of seismic attenuation in the inner core, *Geophys. Res. Lett.*, *31*, L02613, doi:10.1029/2003GL018591.
Ouzounis, A., and K. Creager (2001), Isotropy overlying anisotropy at the top of the inner core, *Geophys. Res. Lett.*, *28*, 4331–4334.
Poupinet, G., R. Pillet, and A. Souriau (1983), Possible heterogeneity of the Earth's core deduced from PKIKP travel times, *Nature*, *305*, 204–206.
Richards, P. (1972), Seismic waves reflected from velocity gradient anomalies within the Earth's upper mantle, *Z. Geophys.*, *38*, 517–527.
Shearer, P. (1994), Constraints on inner core anisotropy from PKP(DF) travel times, *J. Geophys. Res.*, *99*, 19,647–19,659.
Song, X., and D. Helmberger (1995), Depth dependence of anisotropy of Earth' inner core, *J. Geophys. Res.*, *100*, 9805–9816.
Song, X., and D. Helmberger (1998), Seismic evidence for an inner core transition zone, *Science*, *282*, 924–927.
Song, X., and X. Xu (2002), Inner core transition zone and anomalous PKP (DF) waveforms from polar paths, *Geophys. Res. Lett.*, *29*(4), 1042, doi:10.1029/2001GL013822.
Stroujkova, A., and V. Cormier (2004), Regional variations in the uppermost 100 km of the Earth's inner core, *J. Geophys. Res.*, *109*, B10307, doi:10.1029/2004JB002976.
Su, W., and A. Dziewonski (1995), Inner core anisotropy in three dimensions, *J. Geophys. Res.*, *100*, 9831–9852.
Sumita, I., and P. Olson (1999), A laboratory model for convection in Earth's core driven by a thermally heterogeneous mantle, *Science*, *286*, 1547–1549.
Sun, X., and X. Song (2008), Tomographic inversion for three-dimensional anisotropy of Earth's inner core, *Phys. Earth Planet. Inter.*, *167*, 53–70.
Tanaka, S., and H. Hamaguchi (1997), Degree one heterogeneity and hemispherical variation of anisotropy in the inner core from PKP(BC) - PKP (DF) times, *J. Geophys. Res.*, *102*, 2925–2938.
Thomas, C., J.-M. Kendall, and G. Helffrich (2009), Probing two low-velocity regions with PKP b-caustic amplitudes and scattering, *Geophys. J. Int.*, *178*, 503–512.
Tromp, J. (1993), Support for anisotropy of the Earth's inner core from free oscillations, *Nature*, *336*, 678–681.
Vinnik, L., B. Romanowicz, and L. Breger (1994), Anisotropy in the center of the inner core, *Geophys. Res. Lett.*, *21*, 1671–1674.
Vočadlo, L., D. Dobson, and I. Wood (2009), *Ab initio* calculations of the elasticity of hcp-Fe as a function of temperature at inner-core pressure, *Earth Planet. Sci. Lett.*, *288*, 534–538.
Waszek, L., J. Irving, and A. Deuss (2011), Reconciling the hemispherical structure of Earth's inner core with its super-rotation, *Nat. Geosci.*, *4*, 264–267.
Wen, L., and F. Niu (2002), Seismic velocity and attenuation structures in the top of the Earth's inner core, *J. Geophys. Res.*, *107*(B11), 2273, doi:10.1029/2001JB000170.
Woodhouse, J., D. Giardini, and X. Li (1986), Evidence for inner core anisotropy from free oscillations, *Geophys. Res. Lett.*, *13*, 1549–1552.
Yoshida, S., I. Sumita, and M. Kumazawa (1996), Growth model of the inner core coupled with the outer core dynamics and the resulting elastic anisotropy, *J. Geophys. Res.*, *101*, 28,085–28,103.
Yu, W., and L. Wen (2006), Seismic velocity and attenuation structures in the top 400 km of the Earth's inner core along equatorial paths, *J. Geophys. Res.*, *111*, B07308, doi:10.1029/2005JB003995.
Yu, W., and L. Wen (2007), Complex seismic anisotropy in the top of the Earth's inner core beneath Africa, *J. Geophys. Res.*, *112*, B08304, doi:10.1029/2006JB004868.
Yu, W., L. Wen, and F. Niu (2005), Seismic velocity structure in the Earth's outer core, *J. Geophys. Res.*, *110*, B02302, doi:10.1029/2003JB002928.

A. Deuss and L. Waszek, Bullard Laboratories, University of Cambridge, Cambridge CB3 0EZ, UK. (afd28@cam.ac.uk; lw313@cam.ac.uk)